Electron. Mater. Lett., Vol. 11, No. 2 (2015), pp. 187-192
DOI: 10.1007/s13391-014-4327-8

Preparation of Ternary $Cd_{1-x}Zn_xS$ Nanocrystals with Tunable Ultraviolet Absorption by Mechanical Alloying

Qi Zhang,[1] Huihui Zhang,[1] Limin Liu,[1] Shaohua Li,[2] James B. Murowchick,[2] Clarissa Wisner,[3] Nickolas Leventis,[3] Zhonghua Peng,[2,*] and Guolong Tan[1,*]

[1]State Key Laboratory of Advanced Technology for Materials Synthesis and Processing, Wuhan University of Technology, Wuhan 430070, China
[2]Department of Chemistry, University of Missouri-Kansas City, Kansas City, MO 64110, USA
[3]Department of Chemistry, Missouri University of Science and Technology, Rolla, Missouri 65409, USA

(received date: 8 October 2014 / accepted date: 12 November 2014 / published date: 10 March 2015)

Composition-tunable ternary $Cd_{1-x}Zn_xS$ nanocrystals are among the most extensively studied alloyed semiconductor nanocrystals. However, they are almost exclusively prepared by wet chemical routes, which lead to surface-capped nanoparticles. Herein, we present a simple mechanical alloying process to prepare uncapped $Zn_{1-x}Cd_xS$ nanocrystals throughout the entire composition range. The resulting nanocrystals have average sizes smaller than 9 nm, are chemically homogenous, and exhibit linear lattice parameter-composition and close-to-linear band-gap-composition relationships. Continuous lattice contraction of the $Cd_{1-x}Zn_xS$ nanocrystals with the atomic Zn concentration results in a successional enlargement of their band gap energies expanding from the visible region to the ultraviolet (UV) region, demonstrating the ability for precise control of band gap engineering through composition tuning and mechanical alloying.

Keywords: CdZnS, ternary semiconductor, nanocrystals, mechanical alloying, optics

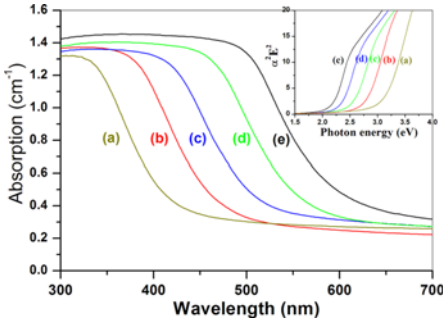

1. INTRODUCTION

Alloyed semiconductor nanocrystals (NCs) enable band gap engineering through both size control and composition tuning.[1-3] Although wet chemical routes have shown to be viable and attractive in preparing alloyed NCs with controlled uniform size and shape,[3-6] mechanical alloying is a far simpler and more versatile technique in preparing composition-tunable NCs.[7-11] Starting from the corresponding elemental powders, chemically homogenous alloyed NCs with sizes less than 10 nm can be prepared by simple mechanical alloying. The composition of the resulting NCs can be precisely controlled by varying the elemental loading ratios. For example, we have recently demonstrated that ternary $CdSe_xS_{1-x}$[12] and $CdTe_xSe_{1-x}$[13] NCs in the entire composition range (x = 0 - 1) can be successfully prepared by mechanical alloying. The ternary CdSeS NCs exhibit strong absorption in the visible range, whereas the CdTeSe NCs extend the absorption to the near infrared (IR) range (up to 1400 nm). Here, we extend the same approach to prepare ternary $Cd_xZn_{1-x}S$ NCs, where the cation atomic compositions are manipulated. The resulting NCs exhibit band gap energies ranging from the ultraviolet (UV) to the visible region depending on the atomic ratio of Cd to Zn.

CdZnS alloys, with direct and wide band gaps ranging from 2.42 to 3.67 eV in their bulk state, are some of the most appealing materials for applications in photonics and optoelectronics.[5,14-18] Their NCs have narrow, tunable, and symmetric emission spectra and are photochemically stable. The band gap of CdZnS NCs is affected more by the composition than the size of the nanocrystals.[19,20] In this work, we report the synthesis of ternary $Cd_xZn_{1-x}S$ NCs, their structural evolution during the mechanical alloying process, and their intrinsic optical spectra.

*Corresponding author: PengZ@umkc.edu
*Corresponding author: gltan@whut.edu.cn

2. EXPERIMENTAL PROCEDURE

High-purity (99.99%) cadmium, zinc, and sulfur powders were purchased from Alpha-Aesar. The raw materials were weighted according to the designed atomic ratio and placed into a stainless steel vial, where stainless steel balls had already been lodged before the elemental powders. Milling balls with various diameters (2 - 12 mm) were used. The ball to powder mass ratio was set to 10:1. The vial was filled with Ar and sealed in a glove box. The vial was then mounted on a SPEX 8000M Mixer/mill machine. During different time intervals of the ball milling, small amounts of as-milled powders were take from the vial in the glove box for structural and optical measurements. The structural evolution of the as-milled powders after different ball milling periods was examined using a Rigaku powder X-ray diffractometer and a JEOL 2100F high-resolution transmission electron microscopy (HRTEM). The optical spectra of the as-milled powders were measured using a Shimadzu UV-3600 UV-VIS-NIR (Ultraviolet-Visible-Near Infrared) spectrophotometer with an ISR3100 integrating sphere attachment.

3. RESULTS AND DISCUSSION

3.1 Structural Evolution upon Mechanical Alloying

Figure 1 presents X-ray diffraction patterns of one mixture (Cd:Zn:S = 0.5:0.5:1) in the early stages of the mechanical alloying process. It is apparent that the diffraction peaks from elemental Cd, Zn, and S dominate the spectrum, indicating that no chemical reactions have occurred within 1 h of the ball-milling process. When the ball milling process was continued for more than 2 h, however, all the elemental diffraction peaks disappeared, as observed in Fig. 2(a), indicating that the mechanochemical reaction of 0.5Cd + 0.5Zn + S → $Cd_{0.5}Zn_{0.5}S$ was completed. Apparently, a rather

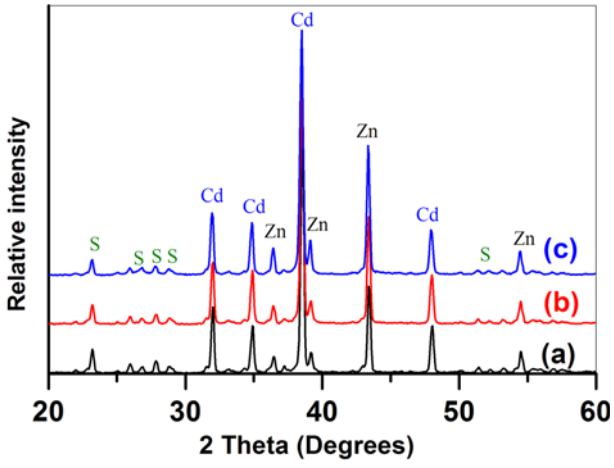

Fig. 1. XRD patterns of the as-milled mixture of 0.5Cd + 0.5Zn + S after milling for (a) 15 min, (b) 30 min, and (c) 60 min.

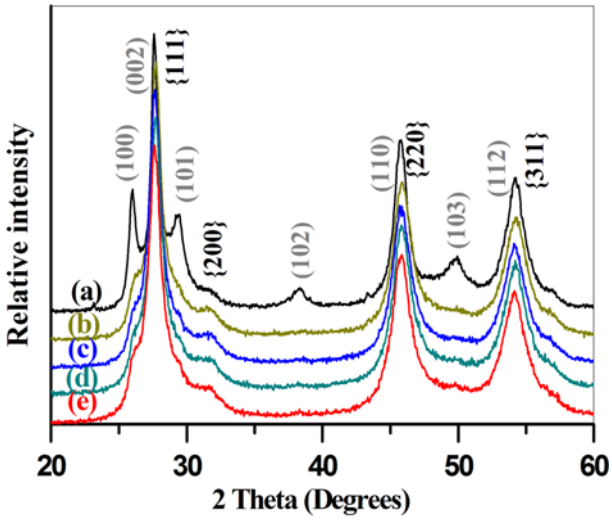

Fig. 2. XRD patterns of the as-milled $Cd_{0.5}Zn_{0.5}S$ compound, which were ball milled for (a) 2 h, (b) 5 h, (c) 10 h, (d) 20 h and (e) 40 h.

long induction period occurs for this particular reaction. All the diffraction peaks in Fig. 2(a) can be indexed to the lattice planes (100), (101), (002), (102), (110), (103), (112), (201) of $Cd_{0.5}Zn_{0.5}S$ crystals in the wurtzite structure.

The XRD patterns of the as-milled $Cd_{0.5}Zn_{0.5}S$ NCs during extended ball milling for as long as 40 h are also presented in Fig. 2, which delineates the continuous structure evolution. When the mechanical alloying process was performed for 5 h, the intensity of the diffraction peak corresponding to the (100) lattice plane in the wurtzite structure decreased significantly, while the diffraction peaks of the (101), (102), and (103) lattice planes disappeared almost completely, as observed in Fig. 2(b). Further prolonging of the ball milling time did not cause any further noticeable change.

The dominant diffraction peaks of the samples collected after extended ball milling for more than 5 h are assigned to the {111}, {200}, {220}, and {311} lattice planes in the zinc blende structure, as shown in Fig. 2. Apparently, the crystal structure of the as-milled $Cd_{0.5}Zn_{0.5}S$ alloys transformed from the wurtzite structure after ball milling for 2 h to a zinc blende structure after 5 h or longer of ball milling. The crystal phase transition is presumably caused by the local high pressure exerted by the milling balls. This phase transition is similar to the high-pressure-induced structural transformation in CdSe nanocrystals.[23] The dominant phase of the final product is the cubic zinc blende structure.

Because the diffraction peak from the (100) lattice planes, albeit weak, clearly remains in the XRD pattern of even the 40-h as-milled $Cd_{0.5}Zn_{0.5}S$ NCs, the existence of a small amount of NCs in the wurtzite structure cannot be excluded. It should be noted that the diffraction peaks from the {111}, {220}, and {311} lattice planes of the zinc blende structure overlap with those from the {002}, {110}, and {112} lattice

planes of the wurtzite structure. The reasonably clean diffraction patterns in Fig. 2 indicate that pure $Cd_{0.5}Zn_{0.5}S$ nanocrystals were successfully fabricated through mechanical alloying of the Cd, Zn, and S elemental powders for more than 5 h. No elemental powders or other impurities are visible in the XRD patterns. The excessive broadening of the {111}, {220}, and {311} diffraction bands reflect the finite size broadening effect. The estimated average particle size for the 40-h as-milled samples is ~9 nm.

The XRD patterns of $Cd_{1-x}Zn_xS$ (x = 0 - 1) NCs with different Cd to Zn mole ratios were studied. All the $Cd_{1-x}Zn_xS$ NCs (x = 0, 0.25, 0.5, 0.75, 1) were ball-milled for 40 h. As observed in Fig. 3, the as-milled CdS NCs have the wurtzite structure,[12] whereas the ZnS NCs have the zinc blende structure.[25] The ternary $Cd_{1-x}Zn_xS$ NCs (x = 0.25, 0.5, 0.75), however, exhibit intermediate structural features with both crystal structure forms coexisting. The $Cd_{0.75}Zn_{0.25}S$ NCs are wurtzite-structure dominant because the diffraction peaks of the (100), (102), and (103) lattice planes are clearly visible in the XRD pattern (Fig. 3b).

The $Cd_{0.5}Zn_{0.5}S$ and $Cd_{0.25}Zn_{0.75}S$ NCs, however, predominantly exhibit the zinc blende structure, as indicated by the disappearance of the diffraction peaks of the (101), (102), and (103) lattice planes of the wurtzite structure (Fig. 3c,d). Even though both the wurtzite and zinc blende structures are observed in the ternary ball-milled NCs, these NCs are clearly chemically homogenous alloys and not heterogeneous mixtures of separate CdS and ZnS nanocrystals, in which case a superposition of the peaks of pure CdS and pure ZnS would be expected. As the Zn content increases, a continuous lattice contraction occurs. A linear relationship is observed between the lattice spacing and cation composition (x), indicating that Vegard's law is followed and again demonstrating the formation of homogeneous alloys. Both

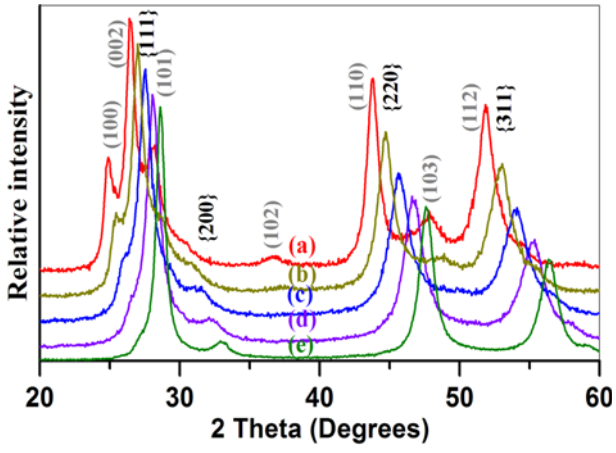

Fig. 3. X-ray diffraction patterns of $Cd_{1-x}Zn_xS$ nanocrystals ball-milled for 40 h: (a) CdS, (b) $Cd_{0.75}Zn_{0.25}S$, (c) $Cd_{0.5}Zn_{0.5}S$, (d) $Cd_{0.25}Zn_{0.75}S$, and (e) ZnS. The grey indices correspond to the wurtzite structure, whereas the black ones correspond to the zinc blende structure.

the chemical composition and varied lattice spacing may contribute to the modulation of the band gap energies of the nanocrystal.

3.2 Microstructures of as-milled $Zn_{0.5}Cd_{0.5}S$ Nanocrystals

The microstructures of as-milled ZnS and CdS NCs have been presented in detail in the literature[24,25] and thus will not be repeated in this paper. Figure 4 presents high-resolution transmission electron microscopy (HRTEM) images of $Cd_{0.5}Zn_{0.5}S$ NCs that were ball-milled for 40 h. Lattice fringes are clearly observed in these images, indicating that the ball-milled alloys are highly crystalline. Consistent with the XRD studies, the majority of the NCs are observed to have the zinc blende structure; however, NCs with the wurtzite structure can also be identified.

For example, particles A, B, C, E, and F encircled in Fig. 4 all have the zinc blende structure, while particle D is identified as a wurtzite structure. The lattice fringes of particles A, B, and C are assigned to the {111} and {200} lattice planes of the zinc blende structure. The spacing for the {111} lattice plane in these zinc blende $Cd_{0.5}Zn_{0.5}S$ nanoparticles is determined to be 3.139 ± 0.015 Å in the fast Fourier transformation (FFT) reciprocal space. The lattice spacing of particle D is determined to be 2.007 Å, which is much smaller than those of other particles and is consistent with the spacing of the (110) lattice planes of a wurtzite $Cd_{0.5}Zn_{0.5}S$ unit cell. The inset shows the FFT pattern of particle E, from which the zone axes of the particle were identified to be zinc blende structure in the [011] orientation. The lattice fringes are assigned to the {111}, {200}, and {311} lattice planes. Small particles (4 - 10 nm) are dominant in these HRTEM images. Larger particles (10 - 20 nm) are also randomly observed.

The as-milled $Cd_{0.5}Zn_{0.5}S$ nanocrystals were subsequently capped with a type of organic-inorganic composite ligand to form a dispersion solution. A small amount of 40-h as-milled powders was placed into a small fresh glass bottle. Then, 5 g trioctylphosphine oxide (TOPO) was melted at 150°C, and 5 mL of trioctylphosphine (TOP) and 0.5 mL of nitric acid (NA) were added to the melted TOPO. Then, 3 - 5 mL of the TOPO/TOP/NA mixture liquid was poured onto the as-milled powders in the glass bottle. A dark-yellow colloid dispersion solution was obtained. Afterwards, 3 mL of pyridine was added into the dispersion solution, which turned into a semi-transparent colorful dispersion solution. The dispersion solution was dropped on a holey carbon transmission electron microscope (TEM) grid for examination by TEM. The TEM and HRTEM measurements were performed on a JEOL 2100F machine.

Figure 5 shows the morphology of the capped $Cd_{0.5}Zn_{0.5}S$ nanocrystals in the dispersion solution. Figure 5(a) presents a low-magnification TEM image of the capped $Cd_{0.5}Zn_{0.5}S$, indicating that the capped $Cd_{0.5}Zn_{0.5}S$ nanocrystals were well

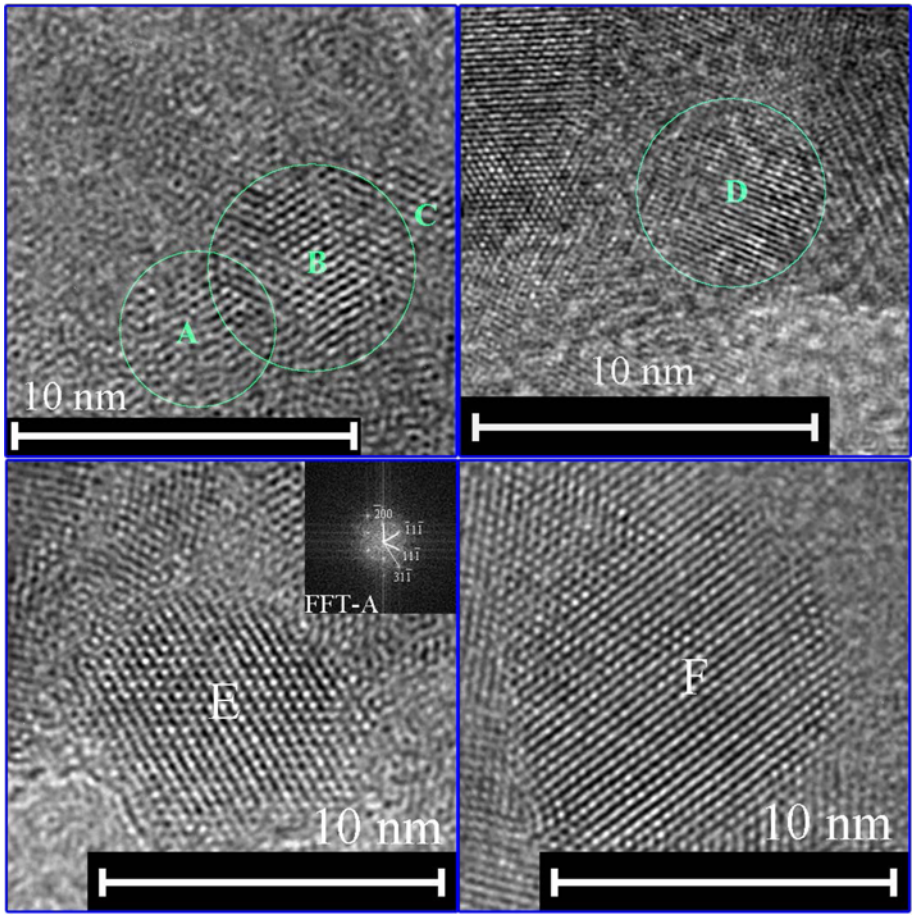

Fig. 4. HRTEM images of the 40-h as-milled $Cd_{0.5}Zn_{0.5}S$ nanoparticles.

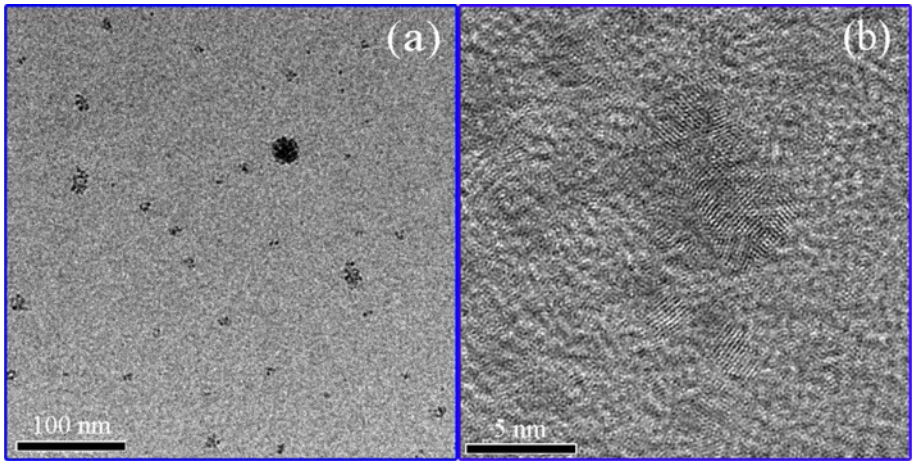

Fig. 5. TEM and HRTEM images of the capped $Cd_{0.5}Zn_{0.5}S$ nanoparticles by TOPO/TOP.

dispersed in the solution. Fig. 5(b) presents an HRTEM image of these capped $Cd_{0.5}Zn_{0.5}S$ nanocrystals, where lattice fringes of {111} planes are clearly observed. These particles exhibit a homogenous size distribution, and no aggregation was observed. The reason for these findings may be that a chemical reaction of TOP + TOPO and NC occurred, which led to the formation of a polymer network. This type of polymer network was extended into the entire dispersion solution; thus, the $Cd_{0.5}Zn_{0.5}S$ nanocrystals were supported by this polymer network, leading to the stable dispersion of $Cd_{0.5}Zn_{0.5}S$ nanocrystals in the solution. The homogeneously distributed nanoparticles in the image suggest that the

dispersibility of the $Cd_{0.5}Zn_{0.5}S$ nanocrystals is good for the spin-coating process and that $Cd_{0.5}Zn_{0.5}S$ nanocrystals are superior for solar cells or thermoelectric materials. The size of the capped $Cd_{0.5}Zn_{0.5}S$ nanocrystals ranged from 2 - 8 nm, with an average size of 4.3 nm.

3.3 Composition-dependent optical properties of as-milled $Zn_{1-x}Cd_xS$ nanocrystals

The absorption spectra of the as-milled uncapped nanocrystals were measured using a Shimadzu UV-3600 UV-VIS-NIR spectrophotometer with an ISR3100 integrating sphere attachment, which allows the direct measurement of powder samples. Figure 6 presents UV-VIS-NIR spectra of the alloyed $Cd_{1-x}Zn_xS$ ($x = 0$ - 1) nanocrystals. All 5 samples were ball-milled for 40 h, such that the samples have similar sizes and size distributions. The as-milled powders were pressed into a round hole (f10 mm) within a sample holder, which was then placed into an integral sphere mounted in a UV-3600 spectrometer. The reflectivity of the alloyed nanocrystals was measured through the integral sphere. The reflectivity was then converted to absorbance using the Kramers-Kronig transformation.

As demonstrated in Fig. 6, a steep decrease in the absorbance at wavelengths near the band gap energy occurred, which is typical for direct semiconductors. The absorbance is very small when the photon energy is less than the band gap energy. However, when the photon energy is higher than the band gap energy, the absorbance increases sharply and steeply. This result reflects the intrinsic band structure of as-milled $Cd_{1-x}Zn_xS$ ($x = 0$ - 1) nanocrystals and is similar to the absorption spectra of bulk semiconductors. These results are consistent with literature reports and our previous research.[12,23,26] As clearly demonstrated in Fig. 6, the absorption edge shifts toward shorter wavelengths when

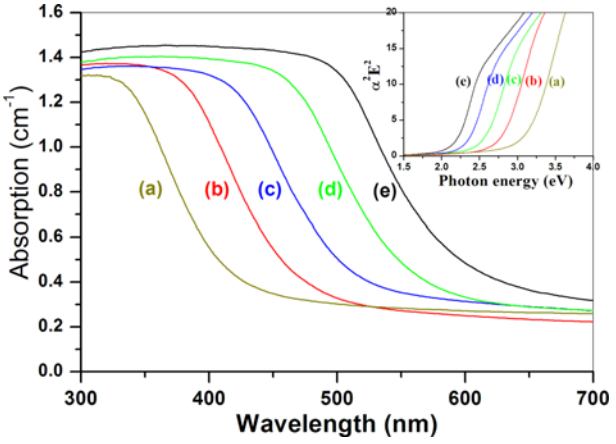

Fig. 6. UV-VIS absorption spectra of 40-h as-milled $Cd_{1-x}Zn_xS$ ($x = 0$ - 1) nanocrystals: (a) ZnS, (b) $Cd_{0.25}Zn_{0.75}S$, (c) $Cd_{0.5}Zn_{0.5}S$, (d) $Cd_{0.75}Zn_{0.25}S$, (e) CdS.

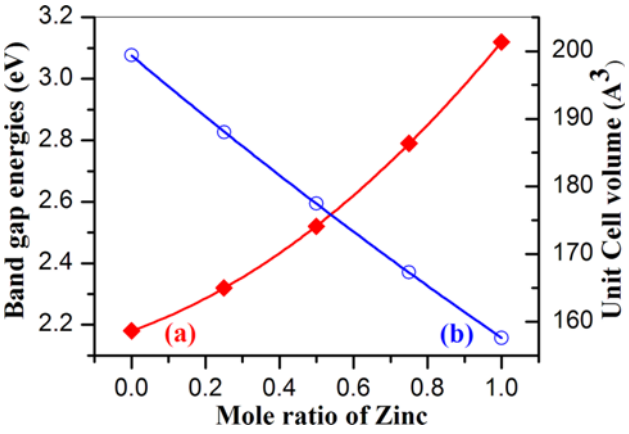

Fig. 7. Dependence of lattice cell volumes (a) and band gap energies (b) of $Cd_{1-x}Zn_xS$ nanocrystals on the Zn content.

the mole fraction of zinc increases.

To extract the band gap energies, a direct gap model using a linear fit to a plot of α^2E^2 versus E in the region of interest was performed, where α is the absorption coefficient in cm^{-1} and E is the photon energy in electronvolts (eV). The plots are shown in the inset of Fig. 6, based on which the band gap energies were obtained by linearly extrapolating the steep α^2E^2 edges to zero absorption. The obtained band gap energies are plotted in Fig. 7(a) (red curve), which clearly demonstrates that the band gap energy increases with increasing mole fraction of Zn in the $Cd_{1-x}Zn_xS$ NCs. The data indicate that the relationship between the band gap energy and the mole fraction x is clearly nonlinear and can be well fitted by the following quadratic equation:

$$E_g(x) = 2.179 + 0.448x + 0.491x^2 \text{ (eV)} \quad (1)$$

This process yields a bowing parameter of 0.49, which is very close to the average bowing constant (0.45) reported in the literature for ternary CdZnS alloys.[27] The band gap energies of the as-milled $Cd_{1-x}Zn_xS$ alloys vary from 2.18 eV (CdS) to 3.12 eV (ZnS) in a nonlinear fashion when x changes from 0 to 1.

As mentioned earlier, the lattice contracts when the Zn content in the alloy increases. As demonstrated in Fig. 7(b), the unit cell volume decreases linearly with the mole fraction x of Zn in $Cd_{1-x}Zn_xS$ NCs. The magnitude of the contraction of the $Cd_{1-x}Zn_xS$ unit cell is 27% when Cd atoms are fully replaced by Zn atoms (or the x value varies from 0 to 1), which is much larger than that of ball-milled $CdSe_{1-x}S_x$, where the lattice contracts only approximately 11%.[12] The much larger difference in ionic size between Zn^{2+} and Cd^{2+} than that between S^{2-} and Se^{2-} may account for the larger cell contraction. The lattice contraction changes the band structure of the nanocrystals and thus should be responsible, at least partially, for the widening of the band gap.

4. CONCLUSION

In summary, pure and homogeneous $Cd_{1-x}Zn_xS$ ($x = 0$ - 1) nanocrystals have been successfully synthesized by mechanical alloying of Cd, Zn, and S elemental powders. The chemical composition of the resulting ternary $Cd_{1-x}Zn_xS$ nanocrystals can be conveniently controlled by the initial loading of the various elements. The average size of the nanocrystals decreases below 10 nm after 40 h of ball milling. As the zinc content in the ternary alloy increases, the crystal structure evolves gradually from the wurtzite structure (CdS, $x = 0$) to the zinc blende type (ZnS, $x = 1$). Meanwhile, the unit cell volume contracts linearly, whereas the band gap increases in a nonlinear fashion. These results unambiguously confirm that chemically homogenous ternary CdZnS alloys with sizes smaller than 10 nm can be conveniently prepared in large quantities by mechanical alloying and that the band gap of the resulting nanoparticles can be tuned by varying the chemical compositions within the UV region. Combined with our previous work on CdSeS and CdSeTe systems, one can envision that alloyed nanocrystals with quaternary or more complicated chemical compositions can be similarly prepared. These uncapped nanocrystals may be superior materials for solar cells or thermoelectric materials.

ACKNOWLEDGEMENTS

The authors acknowledge the financial support received from the Hubei Natural Science Foundation under contract No. 2014CFB166 and the Undergraduate Students' Innovative Foundation of WHUT under contract No. 20141049701018.

REFERENCES

1. M. D. Regulacio and M. Y. Han, *Acc. Chem. Res*. **43**, 621 (2010).
2. L. A. Swafford, L. A. Weigand, M. J. Bowers II, J. R. McBride, J. R. Rapaport, T. L. Watt, S. K. Dixit, L. C. Feldman, and S. J. Rosenthal, *J. Am. Chem. Soc*. **128**, 12299 (2006).
3. A. M. Smith and S. Nie, *Acc. Chem. Res*. **43**, 190 (2010).
4. W. W. Yu and X. G. Peng, *Angew. Chem., Int. Ed*. **41**, 2368 (2002).
5. X. H. Zhong, M. Y. Han, Z. L. Dong, T. J. White, and W. Knoll, *J. Am. Chem. Soc*. **125**, 8589 (2003).
6. J. Tang, S. Hinds, S. O. Kelley, and E. H. Sargent, *Chem. Mater*. **20**, 6906 (2008).
7. P. G. McCormick, T. Tsuzuki, J. S. Robinson, and J. Ding, *Adv. Mater*. **13**, 1008 (2001).
8. Y. Ma, Q. Hao, B. Poudel, Y. C. Lan, B. Yu, D. Z. Wang, G. Chen, and Z. F. Ren, *Nano Lett*. **8**, 2580 (2008).
9. J. L. Guimarães, M. Abbate, S. B. Betim, and M. C. M. Alves, *J. Alloys Compd.* **352**, 16 (2003).
10. M. Achimovičová, K. L. Silva, N. Daneu, A. Rečnik, S. Indris, H. Hain, M. Scheuermann, and H. Hahn, V. Šepelák, *J. Mater. Chem*. **21**, 5873 (2011).
11. B. S. Murty and S. Ranganathan, *Inter. Mater. Rev*. **43**, 101 (1998).
12. G. L. Tan, S. H. Li, J. B. Murowchick, C. Wisner, N. Leventis, and Z. H. Peng, *J. Appl. Phys*. **110**, 1243061 (2011).
13. S. H. Li, G. L. Tan, J. B. Murowchick, C. Wisner, N. Leventis, T. Xia, X. B. Chen, and Z. H. Peng, *J. Electron. Mater*. **42**, 3373 (2013).
14. X. H. Zhong, M. Y. Han, Z. L. Dong, T. J. White, and W. Knoll, *J. Am. Chem. Soc*. **125**, 8589 (2003).
15. X. H. Zhong, Y. Feng, W. Knoll, and M. Y. Han, *J. Am. Chem. Soc*. **125**, 13559 (2003).
16. D. Chen and L. Gao, *Solid State Commun*. **133**, 145 (2005).
17. W. K. Bae, M. K. Nam, K. Char, and S. Lee, *Chem. Mater*. **20**, 5307 (2008).
18. E. Dutkova, P. Balaz, P. Pourghahramani, A. V. Nguyen, V. Sepelak, A. Feldhoff, J. Kovac, and A. Satka, *Solid State Ion*. **179**, 1242 (2008).
19. D. Patidar, N. S. Saxena, and T. P. Sharma, *J. Mod. Opt*. **55**, 79 (2008).
20. Y. K. Liu, C. S. Lee, S. T. Lee, S. L. Shi, and S. J. Xu, *Nanotechnology* **17**, 5935 (2006).
21. S. K. Kulkarnia, U. Winkler, N. Deshmukh, P. H. Borse, R. Fink, and E. Umbach, *Appl. Surf. Sci*. **438**, 169 (2001).
22. S. Sain, S. Patra, and S. K. Pradhan, *J. Phys. D: Appl. Phys*. **44**, 075101 (2011).
23. G. L. Tan, J. H. Du, and Q. J. Zhang, *J. Alloys Compd*. **468**, 421 (2009).
24. G. L. Tan, L. Zhang, and X. F. Yu, *J. Phys. Chem. C*, **114**, 290 (2010).
25. S. Patra, B. Satpati, and S. K. Pradhan, *J. Appl. Phys*. **106**, 034313 (2009).
26. G. L. Tan, N. Wu, J. G. Zheng, U. Hommerich, and D. Temple, *J. Phys. Chem. B* **110**, 2125 (2006).
27. M. C. Tamargo, Ed. Taylor & Francis, New York, Optical Properties and Electronic Structure of Wide Band Gap II-VI Semiconductors, Isaac Hernandez-Calderon in II-VI Semiconductor Materials and Their Applications, 113-170 (2002).